International Journal of Computer Vision and Signal Processing, 11(1), 1-8(2021) ORIGINAL ARTICLE

An Automatic Liver Tumor Detection Method Using Moving Means

Laramie Paxton*

Math and Natural Sciences Department
Marian University–Wisconsin, U.S.A

Yufeng Cao

Keck School of Medicine
University of Southern California, U.S.A.

Kevin Vixie, Yuan Wang

Department of Mathematics & Statistics
Washington State University, U.S.A.

Chaan Ng

M.D. Anderson Cancer Center
University of Texas, U.S.A.

Brian Hobbs

Cleveland Clinic, U.S.A.

Abstract

We present an automatic liver segmentation method that utilizes the time series data in conjunction with the Boykov-Kolmogorov (BK) graph cut algorithm and uses a novel approach of moving means for each of the sample healthy and tumor tissue intensities (from a separate data set) to iterate and improve the initial graph cut segmentation. Thus, there is no training process required since the initial sample means are computed in advance using Regions of Interest provided by radiologists. This method provides a reasonable degree of accuracy for an automatic segmentation scheme, yielding a mean Dice similarity coefficient (DSC) of 77 percent, a relative volume difference (RVD) of 21.6 percent, and a volumetric overlap error (VOE) of 35.7 percent. The algorithm is simple to implement computationally, and the mean runtime of 5.1 minutes is reasonable given that no training process is necessary. The main contribution of this model is to allow the healthy and tumor means to move so that a more optimal segmentation can be obtained.

Keywords: liver tumor, medical imaging, graph cut, segmentation, automatic

IJCVSP

ISSN: 2186-1390 (Online)
http://cennser.org/IJCVSP

Article History:
Received: 7 June 2020
Revised: 28 December 2020
Accepted: 3 February 2021
Published Online: 5 February 2021

1. INTRODUCTION

Liver cancer is a common and deadly disease that requires early detection and treatment options for those afflicted. With the number of new cases increasing rapidly over the past 20 years [1], developing methods to increase detection of the disease and assist in making a proper diagnosis has received considerable attention from the research community. The standard method of identifying liver tumors is for clinicians to examine images manually even as new semi-automatic and automatic tumor detection algorithms have been developed in recent decades. Yet, manual rating is tedious and time-consuming and often varies between and within experts [2]. Thus, we seek a reproducible

*Corresponding author
Email addresses: realtimemath@gmail.com (Laramie Paxton), yufengcaowsu@gmail.com (Yufeng Cao), vixie@speakeasy.net (Kevin Vixie), yuan.wang.stat@gmail.com (Yuan Wang), cng@mdanderson.org (Chaan Ng), hobbsb@ccf.org (Brian Hobbs)

means of liver segmentation that does not depend on clinicians and applies a rigorous method to minimize variation between and within segmentations.

Multi-phase computed tomography (CT) is the most common imaging method used for liver cancer due to its high resolution and speed, but liver tumors themselves exhibit wild variation in overall shape and boundary features with boundaries often being indiscernible from surrounding tissues. What makes the situation even more challenging is that the tumors often have intensities that are very similar to the other healthy or vessel tissues in the liver or nearby anatomical features and organs [3].

In this paper, we propose a significant expansion of the method of automatic liver segmentation presented in [4] that included the use of time series data from the sequence of 59 CT images taken for each patient, as described in [5]. Similar to before, we use a set of sample vectorized means of healthy and tumor tissue intensities from other patients to create a mean of means for each tissue type that can be used in the graph cut in place of any training data for the image we are segmenting. We then fit each of these two (59-dimensional) vector means with a Gaussian B-spline so as to better approximate the actual signals for healthy and tumor tissue intensities prior to using them in the energy functional described below, which the BK graph cut then minimizes for this initial set of vector means. Our new contribution here is to then perturb the coefficients of the Gaussian B-spline of the healthy and tumor mean of means and resample the two (59-dimensional) vector means, hence moving means. We perform the BK graph cut again and repeat this process until the change in energy is less than one percent. This allows for an improved segmentation as shown by the statistical measures in Table 1 below. We also note that there is no training process required since the set of means from other patients can be computed in approximately 5 minutes ahead of time.

The structure of the paper is as follows: First, in Section 2, we present related works and categorize the existing models of liver segmentation. Next, in Section 3, we describe the proposed model in detail along with the statistical evaluations utilized. Lastly, in Section 4, we present and discuss the results of the proposed model.

2. RELATED WORKS

Over the past 20 years, as computer vision techniques have continued to develop greater and greater accuracy, researchers have developed many different methods for the liver segmentation problem, including interactive, semi-automatic, and fully automatic approaches. However, each category of existing models, as described below, still has drawbacks that merit the development of improved models, especially those that handle boundary leakage, low-contrast images, and avoid the necessity of large amounts of training data and lengthy training processes. The motivation of this method is to address these issues by implementing a fully automatic liver segmentation process that does not require training.

One group of common methods for liver segmentation includes region growing [6], [7], clustering [8], [9], and thresholding [10]. These represent some of the earliest approaches to the problem, and while they are computationally straightforward to execute, issues arise on the tumor boundaries since they rely on the intensity of pixels, generally speaking. In recent years, many modified techniques have been proposed such as, adaptive region growing and adaptive thresholding, spatial fuzzy clustering [11], random walkers [12], and the watershed algorithm [13].

Another technique currently making rapid advancement is those based on machine learning, especially convolutional neural networks, which were popularized in the area of liver tumor segmentation by Ronneberger, Fischer, and Brox [14] in 2015. Building upon their method, Christ, et al. [15] employ an approach known as a cascaded fully convolutional neural network. Then in 2019, we saw more developed models such as the deep belief network proposed by Ahmad, et al. [16]. Other examples include [17], [18], [19], [20], and [21]. These methods have achieved promising results in recent years, but tend to have the tradeoff of needing substantial amounts of training data and a rather lengthy training process [22], not to mention the fact that they are more costly computationally speaking.

The third major area of liver tumor segmentation methods is those that rely on energy minimization as a means of segmenting images into healthy, tumor, and sometimes vessel or other types of tissue. These methods can be divided on the one hand into active contour methods [23], [24], [25], such as fast marching and level set [11], and on the other hand graph cuts. Since liver tumor boundaries are often not clearly defined and thus exhibit leaking, active contour approaches have suffered from oversensitization to contour initialization, as the energy minimization process can be disrupted by the presence of local minima [26]. Researchers have thus introduced many different techniques to address these issues, including Markov Random Field level sets [27] and fuzzy clustering [28].

As noted above, the other energy minimization area of extensive research is based on graph cut methods [29], [30], [31], [26], [32], which, unlike the active contour methods mentioned previously, perform the segmentation through a process of global energy minimization. One additional key difference between the two types of methods is that graph cuts are typically not iterative in nature and complete the segmentation in one pass. They also are independent of any contour initializations.

At the heart of the graph cut method is the theory of combinatorial optimization. Suppose we have a connected, undirected graph that we would like to separate into two disconnected pieces. We can represent the graph using pixels as vertices, and we can obtain edges from n-links, which are simply 4- or 8-neighborhood connected groups of pixels. By adding a source and sink to the graph, we can form t-links, which are edges running from each pixel to

both the source and sink nodes [33]. The cut in graph cut refers to the process of minimizing an energy functional by making the minimum-cost cut that produces the two disconnected pieces referred to above.

This energy functional contains a boundary term that involves perimeter regularization and also a regional term corresponding to data fidelity. The boundary term assigns a penalty or cost that is determined by the difference in pixels along boundaries within the image, but it applies only to those edges being cut. On the other hand, the regional term assigns a penalty by classifying pixels within a given region. This is most often done by finding a typical representative pixel or value for a region, such as mean pixel intensity or other measures, and determining the difference between this representative and each surrounding pixel with an appropriate metric, i.e. a function that defines a distance between two given pixels. It should be noted that the metric used in the perimeter term is often different from the one used in the data term due to the situation encountered on the boundaries of tumors and the special consideration needed there.

The underlying mathematical theory that provides the foundation for obtaining the minimization is known as the *Max-flow Min-cut Theorem* [34]. First we define the concept of the cut of minimum capacity to be the smallest overall weight of those edges that, if removed, would disconnect the source and the sink in the network. Loosely speaking, the Max-flow Min-cut Theorem states that if we make the cut of minimum capacity to our flow network, then the weight of all the edges in the cut is equal to the maximal flow that is able to flow through the network.

Perhaps the most well known graph cut algorithm of recent years, which has been used by many different researchers wherever graph cuts are utilized and the one that we use in the proposed method below, is the Boykov-Kolmogorov (BK) max-flow algorithm [35], [36], [37]. While graph cut methods in general tend to exhibit difficulty with noisy images and weak boundaries, such as the leakage described above, many researchers have combined other approaches to address this, for example the random walkers model mentioned previously [12]. Others include an interactive graph cut method using Markov Random Fields and a watershed transform [38] as well as a graph cut method employing fuzzy c-means and a confidence connected region growing algorithm [22].

3. PROPOSED METHOD

3.1. The Energy Functional

Let $F(L)$ below be the energy functional to be minimized in the BK algorithm described above. We segment an image I by clustering the pixels in two clusters around two known means of means from other patients, but we shall penalize for forming too much boundary between the clusters. What we mean here is that we want to avoid the segmentation adding additional, incorrect boundaries in place of the true boundaries. In short, we shall use clustering with predetermined means with both a data fidelity term and a perimeter regularization term, and we let $F(L)$ be minimized over all possible labeling schemes L.

$$F(L) = \sum_i ||I_i - \mu_{L_i}||_2 + \lambda \left(\sum_{\substack{\{i,j \mid L_i \neq L_j, \\ i,j \text{ are neighbors}\}}} \min\{||I_i - I_j||_2^{-1}, 1\} \right). \tag{1}$$

Our two labels $L_i = 1, 2$ are *healthy* and *tumor,* and their cluster centers μ_1 and μ_2 represent the mean of means for each tissue type. Further, we incorporate a normalizing feature for the data term in $F(L)$ such that each term in each sum is between zero and one, allowing us to fix $\lambda \equiv 1$.

We may interpret the first term in the functional as a data fidelity term that computes the 2-norm of the difference between each vectorized pixel and the mean of means for the region it is labeled with. We may interpret the second term in the functional as a perimeter regularization term that computes the edge weight assigned between two pixels that are in different labels. In this case, it is the 2-norm of the difference between any two vectorized pixels along a boundary. This means that perimeter penalties are made only where the edge between two pixels is cut.

The perimeter term is normally large when two pixels p and q are similar in their intensity and is close to zero when the two are very different. One standard form [39] of this term is

$$k \exp\left(-\frac{(I_p - I_q)^2}{2\sigma^2}\right) \cdot \frac{1}{\text{dist}(p,q)}, \tag{2}$$

where $k, \sigma > 0$. In [5], we propose the simpler variant in $F(L)$ above of

$$\min\{||I_i - I_j||_2^{-1}, 1\}. \tag{3}$$

Loosely speaking, it encourages cuts where the norm of the difference of the vectorized pixels is large, such as on ground truth boundaries, and discourages them where this norm is small, with a maximum penalty per cut of one. However, making cuts can become too cheap compared to the data penalty and lead to grainy segmentations, which is why we implement the normalizing component mentioned above for the data term in (1).

3.2. The Dataset

The proposed method was evaluated on a clinical dataset of five hepatic tumors in CT scans from the M.D. Anderson Cancer Center at the University of Texas. Regions of Interest (ROI's) for obtaining the sample tissue mean of

means for healthy and tumor tissues were supplied by experts along with ground truth segmentations. We utilized phase 1 of a 64-stage CT scanner in which a total of 59 slices of 512 × 512 resolution were present in each series taken 0.5 sec apart over 30 seconds. The pixel spacing was either .70 mm or .86 mm, and the slice thickness was 5 mm. Patients were injected with a contrast agent prior to the initial scans. We use the 59th image in each sequence for the segmentation to allow the contrast agent to take its full effect. Note that all computations were performed using Matlab 2020a on a personal computer with 4 GB of RAM and a 2.5 GHz Intel Core i5 CPU.

3.3. Computing the Mean of Means

We begin by vectorizing each pixel p in each of the five other patients using the time series data by which we create a 59-vector for p whose entries consist of the Hounsfield unit (HU) intensities of p at each time step in the sequence. We then extract sample vector means for the tumor and healthy tissues using the ROI's provided by the radiologists. This yields a set of five healthy vector means and five tumor vector means for which we take the mean of each set, yielding a mean of means for both tissue types. We also vectorize each pixel in the image we wish to segment using the time series data. This allows us to include information about the intensity differences over time in the healthy and tumor tissues in addition to the spatial information in the image itself.

3.4. Gaussian B-Spline

Once we have computed the 59-vector mean of means for the healthy and tumor tissues from the other set of patients, we now wish to better approximate the actual signals for these intensities with a continuous function. We therefore fit each set of points using a Gaussian B-spline and then sample these new curves to obtain the 59-vector means μ_1 and μ_2 used in the energy functional $F(L)$ above.

3.5. Moving the Means

After making the initial graph cut using the BK algorithm described previously, we then create a while loop in which we do the following procedure. Having fit each of the 59-vector mean of means for the healthy and tumor tissues with a Gaussian B-spline, we create a 2 × 4 matrix consisting of the four coefficients for each Gaussian of the form

$$f(x) = ae^{-(\frac{x-b}{c})^2} + d.$$

We call this our weight matrix and then proceed to perturb by $\epsilon = .01$ each element in the matrix one at a time. For each perturbation, we then resample the two 59-vector mean of means and run the BK graph cut algorithm again, recording the new energy that results from the algorithm for the functional (1) above. Thus we obtain a 2 × 4 matrix of the new energies that resulted from perturbing each coefficient of the two Gaussians one-by-one.

Next, we subtract the resulting energy of the functional obtained through the initial graph cut from each of the new energies obtained above to get a 2 × 4 matrix of the change in energy of the graph cut that resulted for each perturbation of the coefficients of the Gaussians. We wish to scale this change in energy matrix by the maximum change in energy that occurred for a particular coefficient so as to avoid moving the means too much at once, and so we multiply the matrix by the inverse of this maximum change in energy. Then we subtract this scaled change in energy matrix from the original matrix of coefficients of the two Gaussian curves. This process allows us to adjust the coefficients at each iteration based on the change in energy associated with the perturbation of each coefficient. That is, the bigger the energy change, the more we move that coefficient.

Having moved our vector means and obtained a new weight matrix of coefficients, we then sample them to obtain a new set of 59-vector mean of means for the healthy and tumor tissues based on the associated energy changes in each coefficient. We repeat the graph cut using the BK algorithm and record the resulting energy from the functional $F(L)$ above. If this new energy is larger than the original energy, we cut the elements of the scaled change in energy matrix in half and repeat the sampling process and graph cut algorithm until either the resulting energy is less than the original or the difference between them is less than one percent. If the energy is smaller, the while loop repeats this entire process until the difference between the energy from the current graph cut and the initial is less than one percent.

3.6. Moving Means Steps

Here we present the basic steps for the proposed method. Note that Steps 2-4 can be pre-calculated in approximately 5 minutes.

1. *Begin with the Image, matrix M of vectorized pixels formed using the time series data, and ROI's for computing healthy and tumor sample means from other patients.*
2. *Compute the mean of means (mom) for each tissue type using the time series data.*
3. *Fit each mom to a curve using a Gaussian B-spline.*
4. *Sample the curve to obtain a 59-dimensional vector for each mom.*
5. *Use 8-connectivity to generate an edge weight matrix.*
6. *Generate the terminal weight matrix from M.*
7. *Run BK graph cut.*
8. *Create the weight matrix of Gaussian coefficients.*
9. *Perturb each coefficient, resample the healthy and tumor means, and run BK graph cut.*
10. *Form the change in energy matrix and then scale by the inverse of the maximum change in energy.*
11. *Subtract the scaled change in energy matrix from the original weight matrix.*

12. *Resample the healthy and tumor means, and run BK graph cut.*
13. *If the new energy is larger, scale down the scaled change in energy matrix and repeat the previous step.*
14. *Continue rescaling or repeat the perturbation process until the change in energy is less than 1%.*
15. *Apply liver mask, color scale, and reshape. Obtain segmented image.*

3.7. Evaluation Methods

We use the standard metrics for evaluation as presented in [40].

Volumetric Overlap Error

We divide the number of pixels in the intersection of a segmented tumor (S) and the ground truth (T) by the total number in the union and subtract this result from one to obtain the volumetric overlap error (VOE). A VOE of 0% represents a perfect segmentation.

$$VOE\,(\%) = \left(1 - \frac{|S \cap T|}{|S \cup T|}\right) \times 100 \tag{4}$$

Dice Similarity Coefficient

The Dice similarity coefficient (DSC) is a measure that represents the overall performance of the segmentation. A score of 100% represents a perfect segmentation.

$$DSC\,(\%) = \frac{2|S \cap T|}{|S| + |T|} \times 100 \tag{5}$$

Relative Volume Difference

The relative volume difference (RVD) represents a measure of over- or under-segmentation of a tumor region. It is not a standalone indicator of performance since if the segmented tumor (S) has the same volume as the ground truth (T), a perfect segmentation value of 0% would be reported even if the two regions did not overlap.

$$RVD\,(\%) = \left|\frac{|S|}{|T|} - 1\right| \times 100 \tag{6}$$

4. Results

Table 1 shows the average results performed over a set of five tumors for the proposed method as compared with several other averages for recent automatic segmentation models from the literature. We also include below three segmented images using the proposed method in Fig. 1, Fig. 3, and Fig. 5. In Fig. 2, Fig. 4, and Fig. 6, we show the corresponding ground truth segmentations. Tumor tissue is indicated by yellow.

The proposed method scores well in the DSC metric (77%), which measures the overall performance of the algorithm, and obtains an overall performance higher than five of the other models shown in Table 1. It achieves an RVD of 21.6% and a VOE of 35.7%, both of which are lower, i.e. better, than three of the other models presented, which given the lack of a lengthy training time and the simplicity of the algorithm is promising. These measures could likely be improved by expanding the set of tumors used to form each initial mean of means. Many of the other methods do not report a mean runtime, but the average manual segmentation time is reported to be approximately four minutes per tumor [45].

So while the proposed method's average is 5.1 minutes per image, this is still an acceptable length of time given that the method is fully automatic and there is no lengthy training process involved. To elaborate, the only part of the algorithm in subsection 3.6 that should be precalculated is Steps 1-3 in which we use the ROIs and the set of other patient images to compute a smoothed 59-dimensional vector representing the sample mean of means for both the healthy and tumor tissues using the time series data. This entire process takes only a few minutes. Another important advantage of the proposed method is that

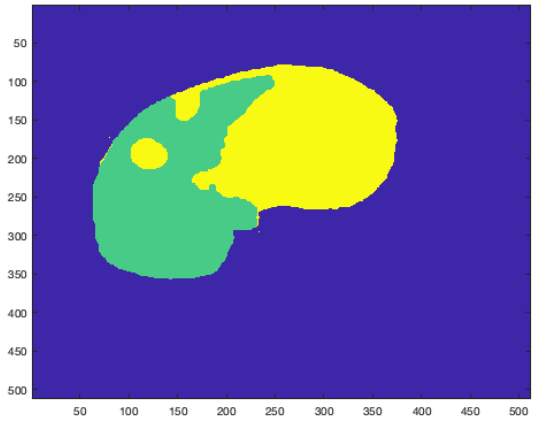

Figure 1: First segmentation result.

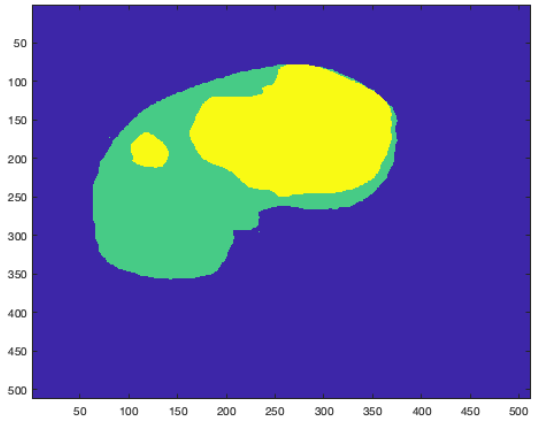

Figure 2: Ground truth segmentation corresponding to Fig. 1.

Table 1: Comparison of Automatic Liver Segmentation Methods

Method	Statistical Measures Reported as Averages			
	VOE (%)	**DSC (%)**	**RVD (%)**	**Run-time (min)**
Masuda et al. [41], 2011	37.2	n/a	30.7	n/a
Linguraru et al. [31], 2012	n/a	74	12.4	50
Huang et al. [42], 2013	32.9	n/a	22.0	n/a
Kadoury et al. [2], 2015	25.2	n/a	14.3	1.7
Ronneberger et al. [14], 2015	39.0	73	87.0	n/a
Christ et al. [15], 2016	16.0	91	6.0	n/a
Moghbel et al. [12], 2016	22.8	75	8.6	0.5
Wu et al. [22], 2017	29.0	83	2.2	0.75
Zeng et al. [43], 2018	33.9	73	n/a	n/a
Gruber et al. [44], 2019	21.8	n/a	9.0	n/a
Paxton et al. [4], 2019	41.5	73	19.5	0.4
Proposed Method	35.7	77	21.6	5.1

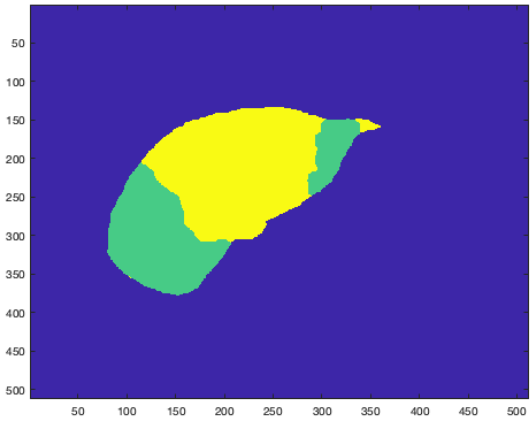

Figure 3: Second segmentation result.

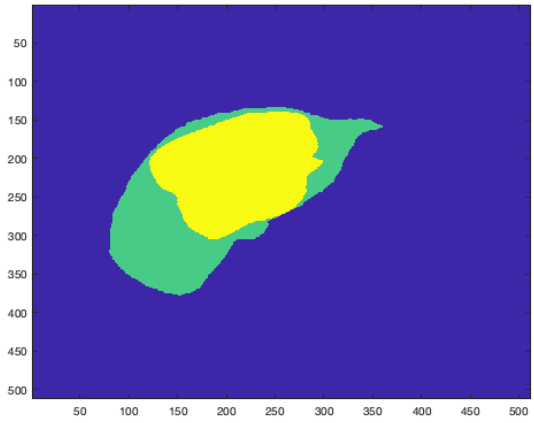

Figure 4: Ground truth segmentation corresponding to Fig. 3.

the algorithm is relatively simple to implement computationally when compared to the other methods shown. The main limitation for the proposed method entails building a suitable set of patient data to form the mean of means for the healthy and tumor tissues in order to more accurately estimate the true population means for each. Improved population mean estimates would likely allow for a more accurate initial segmentation, which would assist the moving means step as well. An additional limitation is when the healthy and tumor intensities in a given patient are very close together in value (e.g. within 5 HU intensity units), which often affects the accuracy of the segmentation even with the moving means component. This occurs, for example, in the third segmentation result shown above in Fig. 5 and in this case results in the second tumor being labeled healthy by the segmentation. However, it is likely that this issue will also be improved by utilizing a larger data set that is more representative of the population means.

5. CONCLUSIONS

We present a fully automatic liver segmentation method that utilizes the time series data in conjunction with the BK graph cut algorithm and a moving means process. As in [5], we vectorize each pixel using the time series data and also make use of the simplified perimeter term in (3) and normalize the data term in the energy functional $F(L)$. We use a set of sample (vector) means of healthy and tumor tissue intensities from other patients to create a mean of means for each tissue type, just as in [4]. There is no training process required since the set of means from other patients can be provided ahead of time based on the ROI's from expert radiologists. We then use a Gaussian B-spline to fit these two vector means to smooth curves as an approximation for the intensity signals for the healthy and tumor tissues. Our contribution is to move these vector means by perturbing the coefficients of the Gaussians and then resampling the two vector means and repeating the BK graph cut, thus allowing for an improved segmentation.

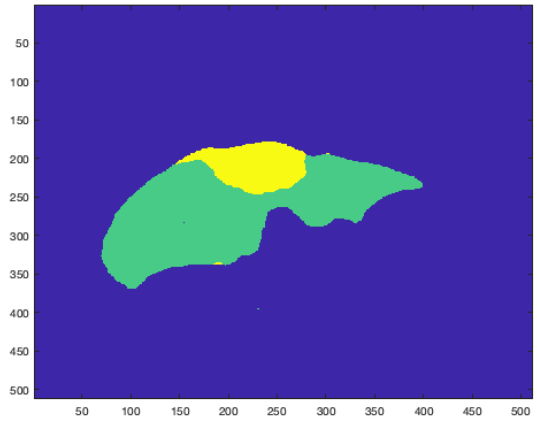

Figure 5: Third segmentation result.

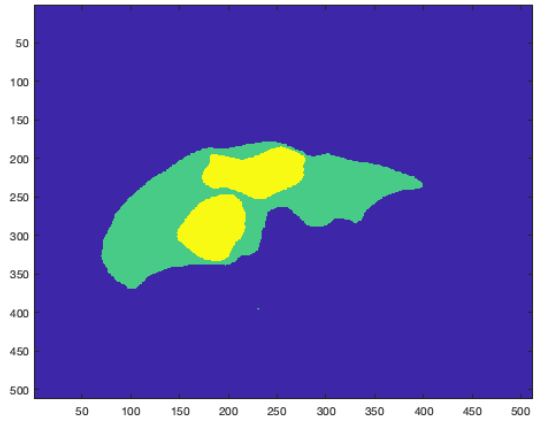

Figure 6: Ground truth segmentation corresponding to Fig. 5.

The method provides a reasonable degree of accuracy for an automatic segmentation scheme, and given that no training process is required, the runtime is also reasonable. Moreover, the algorithm is simple to implement computationally. One area of improvement would be to test the method using a larger set of tumors to form each mean of means so that better representatives of the population means of the healthy and tumor tissue intensity signals could be obtained. It would also be useful to see how the improved estimates for the true population means impact the moving means component.

6. Acknowledgment

This research was partially funded by NIH grant P30-CA016672.

References

[1] U. C. S. W. Group, et al., United states cancer statistics: 1999-2015 incidence and mortality web-based report, US Department of Health and Human Services, Centers for Disease Control and Prevention, and National Cancer Institute.

[2] S. Kadoury, E. Vorontsov, A. Tang, Metastatic liver tumour segmentation from discriminant grassmannian manifolds, Physics in Medicine & Biology 60 (16) (2015) 6459.

[3] R. Rajagopal, P. Subbaiah, A survey on liver tumor detection and segmentation methods, ARPN Journal of Engineering and Applied Sciences 10 (6).

[4] L. Paxton, Y. Cao, K. Vixie, Y. Wang, C. Ng, B. Hobbs, Mean of means: An automatic liver segmentation algorithm, in: 2019 Joint 8th International Conference on Informatics, Electronics & Vision (ICIEV) and 2019 3rd International Conference on Imaging, Vision & Pattern Recognition (icIVPR), IEEE, 2019, pp. 1–5.

[5] L. Paxton, Y. Cao, K. Vixie, Y. Wang, C. Ng, B. Hobbs, A comparison of feature vectors in a graph cut-based liver segmentation algorithm, *Preprint*, 2018.

[6] M. M. Abdelsamea, An automatic seeded region growing for 2d biomedical image segmentation, Proceedings of the International Conference on Environment and BioScience IPCBEE 21.

[7] M. Ganjre, J. Gawande, Automated segmentation of liver and tumour and feature extraction from abdominal CT images using region growing method, in: 10th IRF International Conference, Pune, India, ISBN, 2014, pp. 978–93.

[8] M.-N. Wu, C.-C. Lin, C.-C. Chang, Brain tumor detection using color-based k-means clustering segmentation, in: Intelligent Information Hiding and Multimedia Signal Processing, 2007. IIHMSP 2007. Third International Conference on, Vol. 2, IEEE, 2007, pp. 245–250.

[9] K. Sinha, G. Sinha, Efficient segmentation methods for tumor detection in mri images, in: Electrical, Electronics and Computer Science (SCEECS), 2014 IEEE Students' Conference on, IEEE, 2014, pp. 1–6.

[10] Y. R. Kumar, N. M. Muthukrishnan, A. Mahajan, P. Priyanka, G. Padmavathi, M. Nethra, R. Sneha, M. H. Thakur, Statistical parameter-based automatic liver tumor segmentation from abdominal CT scans: a potiential radiomic signature, Procedia Computer Science 93 (2016) 446–452.

[11] L. Jin-qing, L. Wei-wei, Adaptive medical image segmentation algorithm combined with drlse model, Procedia Engineering 15 (2011) 2634–2638.

[12] M. Moghbel, S. Mashohor, R. Mahmud, M. I. B. Saripan, Automatic liver tumor segmentation on computed tomography for patient treatment planning and monitoring, EXCLI Journal 15 (2016) 406.

[13] A. M. Anter, A. E. Hassenian, Ct liver tumor segmentation hybrid approach using neutrosophic sets, fast fuzzy c-means and adaptive watershed algorithm, Artificial intelligence in medicine 97 (2019) 105–117.

[14] O. Ronneberger, P. Fischer, T. Brox, U-net: Convolutional networks for biomedical image segmentation, in: International Conference on Medical Image Computing and Computer-Assisted Intervention, Springer, 2015, pp. 234–241.

[15] P. F. Christ, F. Ettlinger, F. Grün, M. E. A. Elshaera, J. Lipkova, S. Schlecht, F. Ahmaddy, S. Tatavarty, M. Bickel, P. Bilic, et al., Automatic liver and tumor segmentation of CT and mri volumes using cascaded fully convolutional neural networks, arXiv preprint arXiv:1702.05970.

[16] M. Ahmad, D. Ai, G. Xie, S. F. Qadri, H. Song, Y. Huang, Y. Wang, J. Yang, Deep belief network modeling for automatic liver segmentation, IEEE Access 7 (2019) 20585–20595.

[17] Ü. Budak, Y. Guo, E. Tanyildizi, A. Şengür, Cascaded deep convolutional encoder-decoder neural networks for efficient liver tumor segmentation, Medical hypotheses 134 (2020) 109431.

[18] J. Yang, N. C. Dvornek, F. Zhang, J. Chapiro, M. Lin, J. S. Duncan, Unsupervised domain adaptation via disentangled representations: Application to cross-modality liver segmentation,

in: International Conference on Medical Image Computing and Computer-Assisted Intervention, Springer, 2019, pp. 255–263.
[19] L. Zhang, L. Lu, R. M. Summers, E. Kebebew, J. Yao, Convolutional invasion and expansion networks for tumor growth prediction, IEEE Transactions on Medical Imaging 37 (2) (2018) 638–648.
[20] W. Huang, Y. Yang, Z. Lin, G.-B. Huang, J. Zhou, Y. Duan, W. Xiong, Random feature subspace ensemble based extreme learning machine for liver tumor detection and segmentation, in: Engineering in Medicine and Biology Society (EMBC), 2014 36th Annual International Conference of the IEEE, IEEE, 2014, pp. 4675–4678.
[21] W. Li, F. Jia, Q. Hu, Automatic segmentation of liver tumor in CT images with deep convolutional neural networks, Journal of Computer and Communications 3 (11) (2015) 146.
[22] W. Wu, S. Wu, Z. Zhou, R. Zhang, Y. Zhang, 3d liver tumor segmentation in CT images using improved fuzzy c-means and graph cuts, BioMed Research International 2017.
[23] N. Satpute, J. Gómez-Luna, J. Olivares, Accelerating chan–vese model with cross-modality guided contrast enhancement for liver segmentation, Computers in biology and medicine 124 (2020) 103930.
[24] X. Guo, L. H. Schwartz, B. Zhao, Automatic liver segmentation by integrating fully convolutional networks into active contour models, Medical physics 46 (10) (2019) 4455–4469.
[25] T.-N. Le, H. T. Huynh, et al., Liver tumor segmentation from mr images using 3d fast marching algorithm and single hidden layer feedforward neural network, BioMed Research International 2016.
[26] G. Slabaugh, G. Unal, Graph cuts segmentation using an elliptical shape prior, in: Image Processing, 2005. ICIP 2005. IEEE International Conference on, Vol. 2, IEEE, 2005, pp. II–1222.
[27] A. Raj, M. Jayasree, Automated liver tumor detection using Markov random field segmentation, Procedia Technology 24 (2016) 1305–1310.
[28] B. N. Li, C. K. Chui, S. Chang, S. H. Ong, A new unified level set method for semi-automatic liver tumor segmentation on contrast-enhanced CT images, Expert Systems with Applications 39 (10) (2012) 9661–9668.
[29] Z. Liu, Y.-Q. Song, V. S. Sheng, L. Wang, R. Jiang, X. Zhang, D. Yuan, Liver ct sequence segmentation based with improved u-net and graph cut, Expert Systems with Applications 126 (2019) 54–63.
[30] R. Fang, R. Zabih, A. Raj, T. Chen, Segmentation of liver tumor using efficient global optimal tree metrics graph cuts, in: International MICCAI Workshop on Computational and Clinical Challenges in Abdominal Imaging, Springer, 2011, pp. 51–59.
[31] M. G. Linguraru, W. J. Richbourg, J. Liu, J. M. Watt, V. Pamulapati, S. Wang, R. M. Summers, Tumor burden analysis on computed tomography by automated liver and tumor segmentation, IEEE Transactions on Medical Imaging 31 (10) (2012) 1965–1976.
[32] N. B. S. Vu, Image segmentation with semantic priors: A graph cut approach, Citeseer, 2008.
[33] J. C. Chang, T. Chou, Iterative graph cuts for image segmentation with a nonlinear statistical shape prior, Journal of Mathematical Imaging and Vision 49 (1) (2014) 87–97.
[34] G. Dantzig, D. R. Fulkerson, On the max flow min cut theorem of networks, Linear Inequalities and Related Systems 38 (2003) 225–231.
[35] Y. Boykov, V. Kolmogorov, An experimental comparison of min-cut max-flow algorithms for energy minimization in vision, IEEE Transactions on Pattern Analysis and Machine Intelligence 26 (9) (2004) 1124–1137.
[36] P. Kohli, P. H. Torr, Efficiently solving dynamic markov random fields using graph cuts, in: Computer Vision, 2005. ICCV 2005. Tenth IEEE International Conference on, Vol. 2, IEEE, 2005, pp. 922–929.
[37] P. Kohli, P. H. Torr, Measuring uncertainty in graph cut solutions, Computer Vision and Image Understanding 112 (1) (2008) 30–38.
[38] J. Stawiaski, E. Decenciere, F. Bidault, Interactive liver tumor segmentation using graph-cuts and watershed, in: Workshop on 3D Segmentation in the Clinic: a Grand Challenge II, MICCAI, 2008.
[39] Y. Boykov, M. Jolly, Interactive graph cuts for optimal boundary and region segmentation of objects in nd images computer vision, Proc. 8th IEEE Int. Conf. on Computer Vision ICCV 2001.
[40] A. A. Taha, A. Hanbury, Metrics for evaluating 3d medical image segmentation: analysis, selection, and tool, BMC Medical Imaging 15 (1) (2015) 29.
[41] Y. Masuda, T. Tateyama, W. Xiong, J. Zhou, M. Wakamiya, S. Kanasaki, A. Furukawa, Y. W. Chen, Liver tumor detection in CT images by adaptive contrast enhancement and the EM/MPM algorithm, in: Image Processing (ICIP), 2011 18th IEEE International Conference on, IEEE, 2011, pp. 1421–1424.
[42] W. Huang, N. Li, Z. Lin, G.-B. Huang, W. Zong, J. Zhou, Y. Duan, Liver tumor detection and segmentation using kernel-based extreme learning machine, in: Engineering in Medicine and Biology Society (EMBC), 2013 35th Annual International Conference of the IEEE, IEEE, 2013, pp. 3662–3665.
[43] Y.-z. Zeng, S.-h. Liao, P. Tang, Y.-q. Zhao, M. Liao, Y. Chen, Y.-x. Liang, Automatic liver vessel segmentation using 3d region growing and hybrid active contour model, Computers in biology and medicine 97 (2018) 63–73.
[44] N. Gruber, S. Antholzer, W. Jaschke, C. Kremser, M. Haltmeier, A joint deep learning approach for automated liver and tumor segmentation, arXiv preprint arXiv:1902.07971.
[45] Y. Häme, M. Pollari, Semi-automatic liver tumor segmentation with hidden markov measure field model and non-parametric distribution estimation, Medical Image Analysis 16 (1) (2012) 140–149.